J. Fluid Mech. (2011), *vol.* 679, *pp.* 219–246.
doi:10.1017/jfm.2011.133

On evaporation of sessile drops with moving contact lines

N. MURISIC† AND L. KONDIC‡

Department of Mathematical Sciences, New Jersey Institute of Technology, University Heights, Newark, NJ 07102, USA

(Received 22 June 2010; revised 31 December 2010; accepted 14 March 2011; first published online 18 April 2011)

We consider theoretically, computationally and experimentally spontaneous evaporation of water and isopropanol drops on smooth silicon wafers. In contrast to a number of previous works, the solid surface we consider is smooth and therefore the droplets' evolution proceeds without contact line pinning. We develop a theoretical model for evaporation of pure liquid drops that includes Marangoni forces due to the thermal gradients produced by non-uniform evaporation, and heat conduction effects in both liquid and solid phases. The key ingredient in this model is the evaporative flux. We consider two commonly used models: one based on the assumption that the evaporation is limited by the processes originating in the gas (vapour diffusion-limited evaporation), and the other one which assumes that the processes in the liquid are limiting. Our theoretical model allows for implementing evaporative fluxes resulting from both approaches. The required parameters are obtained from physical experiments. We then carry out fully nonlinear time-dependent simulations and compare the results with the experimental ones. Finally, we discuss how the simulation results can be used to predict which of the two theoretical models is appropriate for a particular physical experiment.

Key words: condensation/evaporation, contact lines, lubrication theory

1. Introduction

A renewed interest for the phenomenon of drying liquid films and drops is due to the rapid advances in semiconductor technologies, and micro- and nano-fluidics. Evaporative sessile drops are particularly interesting due to non-uniform drop thickness and the presence of contact lines, leading to non-uniform evaporation along the liquid–gas interface. The resulting temperature gradients and related Marangoni forces induce flow inside the drop and lead to a number of interesting effects, including contact line instabilities (e.g. see Gotkis *et al.* 2006). These effects are essential in a variety of problems, including the so-called coffee-stain phenomenon which involves deposition of solid particles close to a contact line (Deegan *et al.* 1997; Bhardwaj, Fang & Attinger 2009), and its numerous applications, including the manufacturing and operation of nano- and micro-devices (e.g. see Blossey 2003; Kim *et al.* 2007).

The simplicity of the physical system in which a drop of pure liquid placed on a solid surface evaporates is all but obvious. Yet, much is still unclear, and even systems

† Present address: Department of Mathematics, University of California, Los Angeles, Los Angeles, CA 90095, USA.

‡ Email address for correspondence: kondic@njit.edu

such as drying water drops are not well understood. The most important difference among various models is the manner in which evaporation is introduced into the problem. In addition to usual difficulties in describing the motion of contact lines, evaporation induces a complex interplay between thermal and hydrodynamic effects. Using the appropriate evaporative model is therefore the paramount objective if one is to understand the experiments and the applications which critically depend on the evaporative mechanism.

We devote the opening section to a review of the background to this problem. The review serves as an important motivation for this work, since it illustrates how different assumptions may lead to different (and commonly used) models. We focus on two such models, and outline the mathematical framework in § 3 and the evaporative fluxes in § 4. Section 5 and the Appendix describe experimental techniques employed for estimating volatility parameters. The comparison of predictions of evaporative models directly and against the experimental data in § 6 is the central point of this work.

The issues related to the microscopic physics involved in evaporation next to the contact line are only briefly discussed. Instead, we focus on the scale defined by the drop size, and refer the reader to the literature discussing the relevant micro- and nano-scale physics much more thoroughly (e.g. Israelachvili 1992; Morris 2001). We consider a single solid type (silicon); other solids and a study of the influence of their thermal properties on evaporation are left for future work.

2. Background

The problem of an evaporating drop involves three phases: solid, liquid and gas. Solving the problem in all three phases, coupled with the moving interface problem and the resolution of the flow in the vicinity of the contact line, would be exceedingly complex. Henceforth, we refer the model including 'full' treatment of liquid and gas phases as the two-sided model. Before reviewing simplifications of this model, we discuss the state of the liquid–gas interface and the composition of the gas phase. In thermodynamic sense, either equilibrium (Cachile *et al.* 2002; Hu & Larson 2002, 2005*a*, *b*; Dondlinger, Margerit & Dauby 2005; Haut & Colinet 2005; Margerit, Dondlinger & Dauby 2005; Poulard *et al.* 2005) or non-equilibrium (Burelbach, Bankoff & Davis 1988; Anderson & Davis 1995; Hocking 1995; Ajaev 2005; Sultan, Boudaoud & ben Amar 2005) at the liquid–gas interface is assumed. The gas phase is considered to consists of either vapour itself or a mixture of vapour and inert gas (e.g. air). If we first consider a drop in contact with its vapour only, and that the interface is at thermodynamic equilibrium, the temperature and the pressure in the gas are related through the Clausius–Clapeyron law (Clausius 1850; Atkins & de Paula 2006):

$$\ln\left[\frac{p^*_{sat}}{p^*_0}\right] = \frac{\mathscr{E}_{vap}}{\overline{R}}\left[\frac{1}{T^*_0} - \frac{1}{T^*_{sat}}\right], \tag{2.1}$$

where $\mathscr{E}_{vap}$ and $\overline{R}$ are the enthalpy of vaporization and the universal gas constant, p^*_{sat} and T^*_{sat} are the saturation pressure and temperature, and (p^*_0, T^*_0) is a point on the liquid–vapour co-existence curve. Henceforth, we use the notation $f^* = f[f]$, where f denotes the non-dimensional version of the variable f^*, scaled by $[f]$. The thermocapillary Marangoni effect should not be expected for a drop in contact with its vapour only, unless non-equilibrium is assumed at the interface (Haut & Colinet 2005). On the other hand, the Marangoni effect is more likely to occur when the gas phase is a vapour/inert gas mixture, even under equilibrium assumption, due to possibly large fluctuations of the partial pressure of vapour. Under non-equilibrium assumption, the

mass flux J^* is related to the interface quantities via the Hertz–Knudsen expression from kinetic theory of gases (e.g. Knudsen 1915; Plesset & Prosperetti 1976):

$$J^* = \alpha \sqrt{\frac{M}{2\pi \overline{R} T^*_{sat}}} [p^*_{sat}(T^*_i) - p^*_v], \tag{2.2}$$

where $p^*_{sat}(T^*_i)$ is the saturation pressure at the interface temperature T^*_i, and p^*_v is the vapour pressure just beyond the interface. The parameters α and M are the accommodation coefficient (measuring liquid volatility) and the molecular mass of vapour respectively. Equation (2.2) assumes continuity of temperature across the interface; see Fang & Ward (1999) and Sefiane & Ward (2007) regarding this assumption.

The two-sided model can be simplified by assuming a convection-free vapour/inert gas mixture, and using the fact that vapour viscosity and thermal conductivity are much smaller compared to liquid. This yields a reduction to the Navier–Stokes and energy equations in the liquid, coupled via boundary conditions to the diffusion of vapour in the gas. Various models that follow such an approach are referred to as 1.5-sided models (Dondlinger *et al.* 2005; Haut & Colinet 2005; Margerit *et al.* 2005). These models are still rather complex. In order to simplify further, one may first focus on the vapour concentration, c, satisfying a diffusion equation with vapour mass diffusivity D and appropriate boundary conditions. If the choice of time scale is such that $t_{scale} \gg t_{diff-vap}$, where $t_{diff-vap} = l^2/D$ is the vapour diffusion time scale and l is a typical length scale, the transient term in the diffusion equation can be dropped, simplifying the problem to Laplace's equation: $\Delta c = 0$. Water vapour diffuses into the air with $D \approx 2.5 \times 10^{-5}\ \mathrm{m^2\ s^{-1}}$; using $d_0 = 0.5\ \mathrm{mm}$ as a typical drop thickness and $l \sim d_0$ (to be discussed below) yields $t_{diff-vap} \sim O(10^{-2})\ \mathrm{s}$. In comparison, a sensible choice for t_{scale}, a time scale on which microlitre water drops evaporate, is $\sim O(10^3)\ \mathrm{s}$. Therefore, unless $l \gg d_0$, the reduction to the steady-state formulation is usually appropriate (see Barash *et al.* 2009). Under certain assumptions, most notably of a pinned contact line, this approach leads to an evaporative flux of the form $J \sim h^{-\psi}$, where h is the drop thickness, see Deegan *et al.* (1997, 2000). A similar method, where the diffusion-based evaporative model is coupled with the heat conduction in liquid and solid, was used recently in Dunn *et al.* (2009). Further applications of this approach to problems with pinned contact lines include Popov 2005, Girard *et al.* 2006 and Barash *et al.* 2009. This vapour diffusion-limited evaporation model, henceforth referred to as the 'lens' model, was subsequently extended to problems with moving contact lines, see, e.g. Sefiane, David & Shanahan (2008). In Cazabat & Guena (2010), it was argued that the lens model is generally applicable for isolated drops evaporating in free atmosphere. They listed two possible exceptions: water drops, where the evaporating interface is susceptible to contamination, and situations where thermal conductivities of liquid and solid are comparable, or the liquid is extremely volatile, effectively rendering the stationarity assumption for the vapour concentration inapplicable.

The 1.5-sided model can also be simplified by concentrating on the liquid phase. In this fundamentally different approach, the influence of the gas phase on the evaporative flux is neglected. Such an approach is generally referred to as the one-sided model (Burelbach *et al.* 1988; Colinet, Legros & Velarde 2001). The decoupling of the phases is achieved by assuming that either vapour diffuses rapidly away from the evaporating interface (mixture) or the presence of vapour does not limit the evaporation process (vapour only). The resulting non-equilibrium one-sided model (NEOS) has been used for volatile thin films on heated solid substrates (Burelbach *et al.* 1988) and has been reviewed extensively in Oron, Davis & Bankoff (1997). We

mention here the work by Fischer (2002), where the dependence of the evaporation regime on the environment was studied. Based solely on numerical simulations, it was argued that, depending on the environment, either the lens or the NEOS evaporation model may be utilized. Recent work by Cazabat & Guena (2010) hinted that the NEOS model is relevant for spontaneously evaporating drops surrounded by vapour only or the cases when the evaporating interface is contaminated (e.g. water drops). The NEOS model, under certain assumptions discussed in § 4, leads to an evaporative flux of the form $J \sim 1/(h + \text{const})$.

Some insight regarding a connection between the lens and NEOS models can be gained by examining the relative importance of relevant physical mechanisms. In particular, as in Haut & Colinet (2005), we may consider an evaporation process divided into three distinct steps, each characterized by its own 'resistance': the resistance to phase transition, $\mathscr{R}_p$, the resistance to heat conduction through liquid, $\mathscr{R}_c$, and the resistance to vapour removal by means of diffusion, $\mathscr{R}_d$. The additional resistance due to heat conduction through the solid may also be considered, but we omit it here for brevity. Since there are a number of limiting assumptions, see Haut & Colinet (2005), the argument that follows is meant only to provide an order-of-magnitude estimate. The resistances are defined as follows:

$$\mathscr{R}_p = \frac{\sqrt{2\pi R_g}kT_{sat}{}^{1/2}}{\alpha d_0 c_p p_{air}}, \qquad \mathscr{R}_c = \left.\frac{\mathrm{d}p^*_{sat}}{\mathrm{d}T^*}\right|_{T_s} \frac{d_0 lkL}{c_p p_{air}\left(d_0 lk + {d_0}^2 k_v\right)}, \tag{2.3a, b}$$

$$\mathscr{R}_d = \frac{lkM_{air}}{d_0 M \rho_v c_p D}(1 - N_{up}), \tag{2.4}$$

where $R_g = \overline{R}/M$, k is the liquid thermal conductivity, d_0 is the liquid thickness, c_p is the heat capacity of the liquid, $p_{air} = 1$ atm, L is the latent heat of vaporization and k_v is the thermal conductivity of the vapour (we assume $k_v \approx k_{air}$). Henceforth, the saturation temperature is taken as a parameter in units of temperature. Finally, M_{air}, ρ_v and N_{up} are the molar mass of the inert gas (air), volumetric mass (density) of the vapour and mass fraction of the vapour at the top of the gas layer (ambient value) respectively. The mass fraction of the vapour is given as $N_{up} = \rho_v/(\rho_v + \rho_{air})$, where ρ_{air} is the volumetric mass of air. Using the ideal gas law and the fact that p^*_v, the partial pressure of vapour, may be approximated as $p^*_v \approx H p^*_{sat}(T_{up})$, where H is the relative humidity and $p^*_{sat}(T_{up})$ is the saturation pressure corresponding to T_{up} (ambient temperature), one arrives at the following approximation for N_{up}:

$$N_{up} \approx H \frac{M p^*_{sat}(T_{up})}{M_{air} p_{air}}. \tag{2.5}$$

The derivative in (2.3a, b) is estimated at T_s, the temperature at the liquid–solid interface. Using the Clausius–Clapeyron law, (2.1), the ideal gas law, and the fact that the gas layer is a mixture of air and vapour, this derivative may be approximated as

$$\left.\frac{\mathrm{d}p^*_{sat}}{\mathrm{d}T^*}\right|_{T_s} \approx \frac{L\rho_v N}{T_{sat}}, \tag{2.6}$$

where $\rho_v N$ is the volumetric mass fraction of the vapour in the gas phase. The resistances defined in (2.3a, b) and (2.4) were shown in Haut & Colinet (2005) to

enter the mass flux J corresponding to a composite evaporation model for a volatile liquid film surrounded by a mixture of inert gas and vapour:

$$J = \frac{\dfrac{p^*_{sat}(T_i^*)}{p_{air}} - \dfrac{N_{up}M_{air}}{M}}{\mathscr{R}_p + \mathscr{R}_c + \mathscr{R}_d} \approx \frac{p^*_{sat}(T_{up})}{p_{air}} \frac{1-H}{\mathscr{R}_p + \mathscr{R}_c + \mathscr{R}_d}, \tag{2.7}$$

where the ratio $p^*_{sat}(T_i^*)/p_{air}$ in the numerator drives evaporation, while $(N_{up}M_{air})/M$ suppresses it. The above approximation applies if $p^*_{sat}(T_{up}) \approx p^*_{sat}(T_i^*)$.

If a particular resistance is small, the corresponding step in the evaporation process may be ignored. For example, if $\mathscr{R}_p \ll \mathscr{R}_d$, the evaporating interface is at local thermodynamic equilibrium; if $\mathscr{R}_c \ll \mathscr{R}_d$, the heat is supplied to the interface relatively fast, but the phase transition is negligible due to the relatively slow rate of vapour removal, and hence the interface is at room temperature (non-volatile case); finally, if $\mathscr{R}_d \ll \mathscr{R}_c$, the diffusion of vapour away from the interface is rapid, and therefore the composition of the gas phase is uniform. As a result, several crucially different evaporation regimes emerge: if $\mathscr{R}_p \gg \mathscr{R}_c, \mathscr{R}_d$, evaporation is reaction-limited and the interface is at non-equilibrium (as in the NEOS model); if $\mathscr{R}_c \gg \mathscr{R}_p, \mathscr{R}_d$, evaporation proceeds in the heat conduction-limited regime and the interface is at thermodynamic equilibrium; if $\mathscr{R}_d \gg \mathscr{R}_p, \mathscr{R}_c$, the limiting mechanism is vapour diffusion (as in the lens model), with interface also in equilibrium.

The expression for $\mathscr{R}_p$ has roots in the kinetic theory of gases. Among other quantities, $\mathscr{R}_p$ depends on the accommodation coefficient α, which describes the probability of phase change. However, the α used in the literature vary across several orders of magnitude: $O(10^{-6})$–$O(1)$. In particular, while in Kennard (1938) it was argued that α should be small, $\alpha = 1$ was used in Schrage (1953) and Sultan *et al.* (2005), $\alpha = 0.83$ in Burelbach *et al.* (1988), and $\alpha = 0.1$ in Colinet *et al.* (2001). The theoretical predictions suggested that $\alpha \in [10^{-2}, 1]$ for water (Marek & Straub 2001). Nevertheless, these predictions were found to overestimate the volatility and have failed to agree with the experiments – in fact, values of α in the range $O(10^{-6})$–$O(10^{-2})$ have been measured (Mansfield 1955; Derjaguin, Fedoseyev & Rosenzweig 1966; Barnes 1978; Marek & Straub 2001). While particularly small values ($O(10^{-6})$–$O(10^{-5})$) resulted from experiments with water drops where the surface was intentionally contaminated by monolayers of cetyl alcohol (Mansfield 1955; Derjaguin *et al.* 1966), susceptibility of water, in particular, to unintentional contamination by surfactants has been identified as one of the main reasons for small measured values of α (Cammenga 1980; Barnes 1986). Effectively, for water, the values of α in the range $[10^{-2}, 1]$ may be measured only in experiments carried out in vacuum or when the evaporating surface is continuously renewed (Cazabat & Guena 2010). When water drops are allowed to evaporate in free atmosphere without manipulating (i.e. renewing) the evaporating surface, $\alpha \leqslant O(10^{-4})$ is likely to result (Murisic & Kondic 2008; Cazabat & Guena 2010). We note that the range $[10^{-6}, 1]$ for α leads to a wide range of values of $\mathscr{R}_p$, as illustrated in table 1.

The resistance $\mathscr{R}_c$, (2.3*a*, *b*), measures the relative importance of heat conduction in liquid with respect to the one in the gas phase. While most of the parameters entering (2.3*a*, *b*) and (2.6) are well known, the relevant extent of the gas phase, l, is difficult to estimate. While l only weakly influences $\mathscr{R}_c$, it strongly modifies $\mathscr{R}_d$, as illustrated in table 1, where we use $H = 0.5$ and consider the values of l varying between $80d_0$, suggested by Hu & Larson (2002), and $0.1d_0$, which may be relevant in the case of drops open to the atmosphere where the vapour can also be removed by convection

l	α	$\mathscr{R}_p$	$\mathscr{R}_c$	$\mathscr{R}_d$	Evaporation limited by, appropriate model
$0.1d_0$	10^{-4}	0.26×10^2	0.41	0.92	Volatility, NEOS
d_0	10^{-4}	0.26×10^2	0.56	0.92×10^1	Volatility + vapour diff., mixed
$80d_0$	10^{-4}	0.26×10^2	0.59	0.74×10^3	Vapour diff., lens
$80d_0$	10^{-1}	0.26×10^{-1}	0.59	0.74×10^3	Vapour diff., lens
d_0	10^{-1}	0.26×10^{-1}	0.56	0.92×10^1	Vapour diff., lens
$0.1d_0$	10^{-1}	0.26×10^{-1}	0.41	0.92	Vapour diff. + heat cond., mixed

TABLE 1. Table of the values of resistances relevant to the evaporation process for water, relative to the choice of values for l and α.

in the gas. Table 1 summarizes the effect of changing α and/or l, illustrating how these parameters may lead to a transition between different evaporation regimes.

To summarize, the choice of the relevant evaporation model depends on the quantities that cannot be estimated precisely, such as the relevant gas phase thickness, l, or for which a range of results exist, such as the accommodation coefficient, α. As pointed out e.g. in Haut & Colinet (2005) and Cazabat & Guena (2010), even when the gas phase is an inert gas/vapour mixture, additional information about the set-up is required before one can decide which model is more appropriate. In this paper, we expand on the preliminary results of the numerical study of evaporation models (Murisic & Kondic 2008) and show how physical experiments, combined with modelling and simulations, can be used to distinguish between the two commonly used evaporation models. We discuss the differences between these models and compare their predictions directly and against our experimental results. To the best of our knowledge, this is the first time such a comparison has been carried out using data appropriate to a particular experiment.

3. Problem formulation

The main building blocks of the model are as follows:

(i) the spreading drop is characterized by a small aspect ratio so that lubrication approximation is appropriate;

(ii) Marangoni forces are considered, so that the dependence of surface tension on temperature is included;

(iii) the effect of the thermal conductivity of the solid and liquid phases as well as the vapour recoil effect is included;

(iv) the solid–liquid interaction is modelled using a disjoining pressure approach.

The solid–liquid interaction is included through a model with both attractive and repulsive terms which are often considered to result from van der Waals (vdW) intermolecular forces, leading to a stable equilibrium liquid layer. We note that we focus on pure liquids; the Marangoni effect arising due to the variation in liquid composition is hence neglected. That thermocapillary Marangoni effect is relevant even for water drops was shown in the experiments carried out by Xu & Luo (2007).

The starting point of the model is the Navier–Stokes equations, accompanied by the energy equations (liquid and solid) and, in general, by the diffusion equation for vapour. Figure 1 shows the physical set-up. Our model derivation mostly follows the approach presented in Burelbach *et al.* (1988), with a few modifications which are relevant to the present work. In particular, we keep the evaporative flux unspecified at this point, so that later we will be able to apply either the lens or the NEOS model.

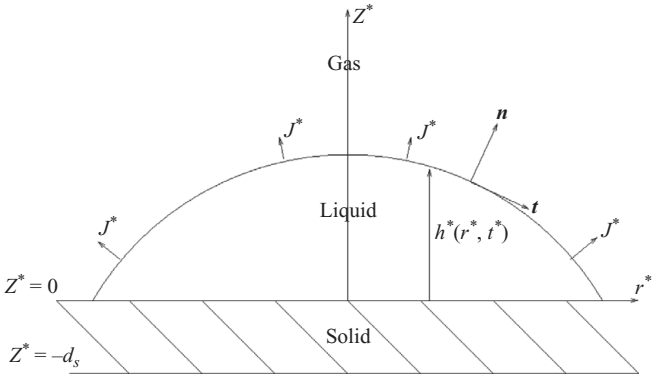

FIGURE 1. The physical configuration: the evaporating drop on a horizontal solid surface.

Moreover, to account for vdW forces, we include a disjoining pressure model, allowing us to carry out time-dependent simulations of the resulting equation. An inclusion of such a term has been reviewed in e.g. Oron *et al.* (1997) and discussed by other authors in the presence of evaporation (Colinet *et al.* 2001; Ajaev 2005). The temperature at the bottom of the solid layer is prescribed as $T_s^*(-d_s, t^*) = T_0$, where T_0 is the reference (room) temperature. This particular choice is appropriate for our experimental set-up, where a solid wafer rests on an insulating platform at a fixed (room) temperature. At the liquid–solid boundary, $z^* = 0$, we assume no-slip and no-penetration conditions, along with continuity of the temperature and matching heat fluxes between the liquid and the solid. We use the scales similar to those in Burelbach *et al.* (1988): d_0 is the length scale ($\sim$0.5 mm, typical drop thickness); d_0^2/ν, ν/d_0 and $\rho\nu^2/d_0^2$ are the viscous scales for time, velocity and pressure respectively (ν and ρ are the kinematic viscosity and density of liquid); the scale for the evaporative mass flux is $k\Delta T/(d_0 L)$; finally, the temperature difference $T_i^* - T_{sat}$ is scaled against $\Delta T = T_0 - T_{sat}$. Since we assume that the aspect ratio of the drop is small, we employ the lubrication approximation in order to simplify our model. Within the lubrication approximation, the final equation for the thickness, $h = h(r, t)$, of an axisymmetric volatile drop in polar coordinates (see Murisic & Kondic 2008) is given by

$$\frac{\partial h}{\partial t} + EJ + \frac{S}{r}\left[rh^3\left(h_{rrr} + \frac{1}{r}h_{rr} - \frac{1}{r^2}h_r\right)\right]_r - \frac{E^2}{rD}[rh^3 J J_r]_r + \frac{Ma}{rP}[rh^2[(h + \mathscr{W})J]_r]_r + \frac{A}{r}\left[rh^3\left(\left(\frac{b}{h}\right)^3 - \left(\frac{b}{h}\right)^2\right)_r\right]_r + \frac{G}{r}[rh^3 h_r]_r = 0. \tag{3.1}$$

The consecutive terms describe viscous dissipation, evaporation, capillary effects, vapour recoil, the Marangoni effect, disjoining pressure and gravity respectively. The disjoining pressure term involves an (n, m)-type potential, see e.g. Schwartz & Eley (1998) and Diez & Kondic (2007). The non-dimensional parameters appearing here, defined as

$$E = \frac{k\Delta T}{\rho\nu L}, \quad S = \frac{\sigma_0 d_0}{3\rho\nu^2}, \quad D = \frac{3\rho_v N}{2\rho}, \quad Ma = \frac{\gamma\Delta T d_0 c_p}{2\nu k}, \quad P = \frac{\nu\rho c_p}{k}, \tag{3.2}$$

are the evaporation number, scaled surface tension, density ratio, and Marangoni and Prandtl numbers respectively. We note that σ_0 is the surface tension at room

Parameter	Water	Isopropanol	Non-dim. Par.	Water	Isopropanol
T_{sat} (K)	286.8	256.1	D	10^{-5}	10^{-5}
$\rho_v N$ (kg m^{-3})	1.196×10^{-2}	7.549×10^{-3}	E	10^{-3}	10^{-3}
ρ (kg m^{-3})	998	790	Ma	10^{3}	10^{4}
γ (N K^{-1} m^{-1})	0.18×10^{-3}	0.25×10^{-3}	A	10^{6}	10^{3}
σ_0 (N m^{-1})	7.2×10^{-2}	2.1×10^{-2}	$\lvert G\rvert$	10^{2}	10^{1}
L (J kg^{-1})	2.44×10^{6}	0.79×10^{6}	S	10^{4}	10^{2}
R_g (J kg^{-1} K^{-1})	461.92	138.35	$\mathscr{K}$	10	1
ν (m^2 s^{-1})	0.902×10^{-6}	2.582×10^{-6}	P	1	10
k (W K^{-1} m^{-1})	6.05×10^{-1}	1.35×10^{-1}	$\mathscr{W}$	1	1
k_s (W K^{-1} m^{-1}) (Si)	1.35	1.35			
c_p (J kg^{-1} K^{-1})	4.18×10^{3}	2.4×10^{3}			

TABLE 2. Table of parameter values (left) and non-dimensional parameters (right) at $T = 298$ K for water and isopropanol (Lide 1997).

temperature, and $\gamma = -\mathrm{d}\sigma/\mathrm{d}T > 0$ for most liquids. Also

$$\mathscr{W} = \frac{k d_s}{k_s d_0}, \qquad A = \frac{\Omega d_0}{3\nu^2 \rho \mathscr{N} b}, \qquad G = -\frac{d_0^3 g}{3\nu^2}, \tag{3.3}$$

where $\mathscr{W}$ describes the thermal effects in the solid: $d_s = 0.75$ mm is the typical thickness and k_s is the thermal conductivity of silicon wafers. Furthermore, $b = d_{equil}/d_0$, where d_{equil} is the equilibrium film thickness (resulting from disjoining pressure), $\Omega = \sigma_0(1 - \cos\Theta)$ and $\mathscr{N} = (n - m)/((n - 1)(m - 1))$. We use $(n, m) = (3, 2)$, see Schwartz & Eley (1998), and note that the results do not depend in any significant manner on this choice. Finally, g is the gravitational acceleration, and Θ is the contact angle. The non-dimensional parameter A therefore encodes the contact angle behaviour; we note that here both A and b are independent of the liquid temperature.

Before specifying the evaporative flux, it is appropriate to briefly discuss the values of the non-dimensional parameters appearing in (3.1) for the physical problems of interest. Table 2 lists the values of the most important material parameters. We concentrate on two types of pure liquids with substantially different volatilities at room conditions – water and isopropanol (alcohol) – and silicon (Si) solids. T_{sat} is obtained from the Clausius–Clapeyron law, (2.1): we consider $(p_0, T_0) = (1\,\text{atm}, 355\,\text{K})$ for isopropanol and (1 atm, 373 K) for water (normal boiling points for the two liquids). For representative values of 50 % relative humidity (water) and 5 % relative vapour content in the surrounding gas (isopropanol), we obtain $p_{sat} = 1.58$ kPa for water and $p_{sat} = 267$ Pa for isopropanol; these are then used in the Clausius–Clapeyron law to calculate T_{sat} for water and isopropanol. The $\rho_v N$ values from table 2 are calculated from the ideal gas law, using p_{sat} and T_{sat}. The choice of values for relative humidity and vapour content has only a minor influence on the results – e.g. if relative humidity (vapour content) is varied between 40 % and 60 % (2 % and 10 %), calculated T_{sat} changes by only 1 %.

Table 2 also gives the order-of-magnitude size of relevant non-dimensional parameters for both water and isopropanol. We note that our assumptions regarding the relative size of dependent parameters have been extensively used in previous studies (e.g. see Burelbach *et al.* 1988; Oron *et al.* 1997; Craster & Matar 2009). In addition to allowing retainment of all physical mechanisms at the leading order in

our model, these assumptions also ensure regularization of the resulting governing equation by maintaining the high-order capillary term.

4. The two evaporation models

The two evaporation models we consider have been extensively reviewed in the Introduction. Here, we discuss the precise formulation of the evaporative flux needed for our simulations and comparison with experiments.

4.1. *The lens evaporation model*

The lens model is consistent with the liquid–gas interface at equilibrium and the evaporation limited by the diffusion of vapour into the surrounding gas. The problem for vapour mass diffusion is reduced to Laplace's equation for vapour concentration, c^*, accompanied by the boundary condition at the liquid–vapour interface (constant saturation concentration) and some far-field condition (ambient concentration). If the drop is assumed to be a spherical cap, this boundary value problem has an electrostatic equivalent: the problem of finding an electric field exterior to a lens-shaped conductor, where c^* is equivalent to the electrostatic potential and the mass flux J^* to the electric field (Picknett & Bexon 1977; Deegan *et al.* 1997). An additional requirement is that there should be no evaporation beyond the contact line of the drop. Solving this electrostatic problem analytically is rather complex (Deegan *et al.* 2000; Popov 2005), but the resulting expression for the mass flux J^* can be well approximated by (Hu & Larson 2002)

$$J^*(r^*) = \frac{J_{lens}}{(R^2 - r^{*2})^{\lambda}}, \tag{4.1}$$

where R is the drop radius, r^* is the radial distance from the drop centre and J_{lens} is an evaporation coefficient to be related to the volatility parameter below. We use the expression $\lambda = 1/2 - \Theta/\pi$ from Hu & Larson (2002), which achieved the best fit between the approximation, (4.1), and the numerical solution for J^* (obtained from the numerical solution for c^*, using the boundary condition $J^* = D\nabla^* c^*$ at the evaporating interface); it was found to be valid for $\Theta \in [0, \pi/2]$, with the maximum relative error $<6\,\%$. We note that the results in Hu & Larson (2002) depend on the choice of the relevant thickness of the gas phase, l. In particular, if $l \ll 80 d_0$, e.g. $l \sim d_0$, the validity of the vapour diffusion-limited evaporation model and (4.1) become questionable, as discussed in § 2.

In what follows, we assume that the surface of the drop is well approximated by a spherical cap, see figure 2, an assumption discussed in more detail later in § 5. Here, we only note that this approach is justified by a small relevant capillary number, $Ca = \mu^2/(\rho\sigma_0 d_0) \sim O(10^{-4})$, and a small Bond number, $Bo = (\rho g {d_0}^2)/\sigma_0 \sim O(10^{-2})$. Hence, the thickness of the drop is $h^* = \sqrt{R^2 + d^2 - r^{*2}} - d$, where $d = (R^2 - {d_0}^2)/(2d_0)$. Since the shape of the drop changes slowly, R and d_0 are treated as constants. Next, we non-dimensionalize (4.1), using $[J] = (k\Delta T)/(d_0 L)$. Substituting the expression for $r = r^*/d_0$ in terms of $h = h^*/d_0$ gives

$$J(h) = \frac{J_{lens}}{[J] {d_0}^{2\lambda} (h((R/d_0)^2 - 1 + h))^{\lambda}}. \tag{4.2}$$

For small Θ, the dominant term in the brackets is $(R/d_0)^2$, allowing the reduction to

$$J(h) = \frac{\chi}{h^{\psi}}, \tag{4.3}$$

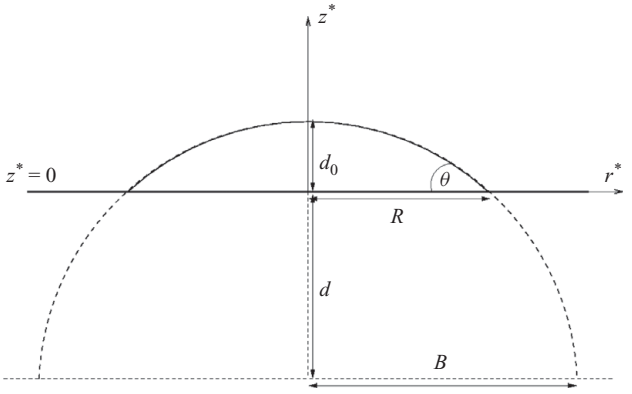

FIGURE 2. The spherical cap approximation.

where $\psi = \lambda$. The volatility parameter χ is given as $\chi = J_{lens}/([J]R^{2\lambda})$. For larger Θ (i.e. $R \sim d_0$), (4.3) is still valid, but with $\psi = 2\lambda$ and $\chi = J_{lens}/([J]{d_0}^{2\lambda})$. We note that here J diverges as $h \longrightarrow 0$. Although this divergence is integrable, it is not physical. However, in the approach we use, the disjoining pressure naturally removes this divergence, by introducing a length scale, related to d_{equil}, where evaporation stops due to attractive vdW forces. The manner in which χ is determined experimentally is discussed in § 5.

4.2. *The NEOS evaporation model*

This model corresponds to a case when $\mathscr{R}_p \gg \mathscr{R}_c, \mathscr{R}_d$ (reaction-limited evaporation with the interface at non-equilibrium). The decoupling of the liquid and gas phases allows us to solve the problem in the liquid phase only and ignore the vapour. The mass flux J satisfies the Hertz–Knudsen relation, (2.2). We note that while (2.2) was originally introduced in Knudsen (1915) for evaporation of pendant drops, it typically requires correction for the Laplace pressure when describing evaporation from curved interfaces, see e.g. Ajaev (2005). Here, this correction is small – $O(10^{-5})$ – hence, we neglect it, similarly to Cazabat & Guena (2010), where sessile drops were also considered. The Clausis–Clapeyron law, (2.1), is used to relate the temperature and the pressure, and thus we obtain the boundary condition at the liquid–gas interface:

$$J^* = (T_i^* - T_{sat}) \left(\frac{\alpha L \rho_v N}{T_{sat}^{3/2}} \right) (2\pi R_g)^{-1/2}. \tag{4.4}$$

The use of the scales for temperature and evaporative mass flux gives $J = T/\mathscr{K}$. The non-equilibrium parameter $\mathscr{K}$ is given by

$$\mathscr{K} = \frac{(2\pi R_g)^{1/2} k T_{sat}^{3/2}}{\alpha d_0 L^2 \rho_v N}. \tag{4.5}$$

Using the connection between the temperature and the evaporative flux at $z = h$ as in Burelbach *et al.* (1988) gives

$$J(h) = \frac{1}{h + \mathscr{K} + \mathscr{W}}. \tag{4.6}$$

For water, $\mathscr{K} + \mathscr{W} \sim O(10)$; hence, $J(h)$ depends only weakly on h. Furthermore, J in (4.6) remains finite as $h \longrightarrow 0$, unlike the one in (4.3).

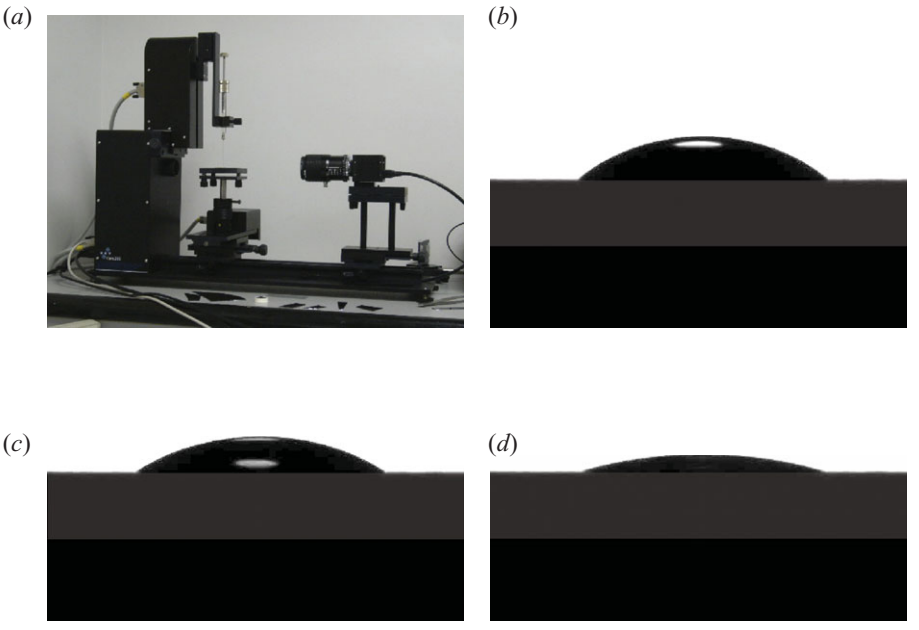

FIGURE 3. (Colour online available at journals.cambridge.org/FLM) (*a*) The goniometer: camera, syringe and deposition platform. Snapshots of the evaporating water drop recorded at (*b*) 56 s, (*c*) 256 s and (*d*) 536 s. The silicon wafer is shown in grey; the drop itself and goniometer platform are black.

Depending on which evaporation model is considered, J given by either (4.3) or (4.6) may be substituted into (3.1), which can then be solved numerically, provided volatility parameters are known. Therefore, we proceed by describing our experiments carried out in order to find the unknown volatility parameters χ and α.

5. The experimental procedure

The main goal of the experiments is twofold: first, they provide the data for the rate of mass loss and allow us to estimate χ and α; second, the experimental data regarding the evolution of the drop volume and the position of the contact line provide a benchmark for the two theoretical models.

We carry out the experiments using a goniometer (KSV CAM 200), which consists of a camera, light source, static deposition platform and a Hamilton 1700 Series GASTIGHT syringe (see figure 3*a*); also included is image analysis software. The experiments are performed at room temperature and in open atmosphere. While we impose no special precautionary measures to shield the experimental set-up from sources of air convection, we examine the influence of applied convection on experimental data and find it to be insignificant (see the discussion accompanying figure 10 in § 6.1).

In the experiments, water and isopropanol drops are deposited onto smooth semiconductor grade Si wafers, treated by chemical–mechanical polishing that reduces surface roughness (Rms) to 0.5 nm (the same wafers as in Gotkis *et al.* 2006 are used). No additional preparation or cleaning of wafers is employed. We note that rapid oxidation of Si wafers can lead to formation of hydroxyl groups and siloxane bridges – our experimental results showing a well-defined initial contact angle for water $\approx 40.9^\circ$,

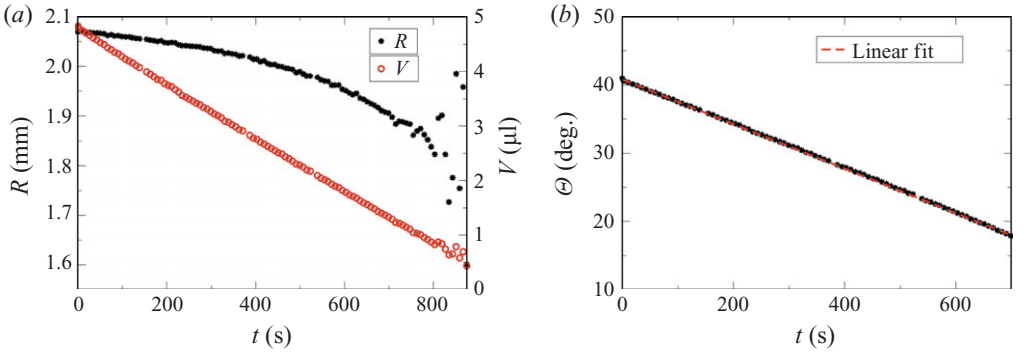

FIGURE 4. (Colour online) (*a*) Evolution of the volume and radius of a drop of water. (*b*) Evolution of the contact angle Θ for a drop of water during the interval $[0, t_f]$. The linear fit $\Theta(t)$ (dashed line) is used in our theoretical model. The size of symbols accounts for the experimental error.

see figure 4(*b*), suggest that the siloxane bridges dominate and that the surface is reasonably homogeneous (we thank an anonymous referee for providing further insight regarding this issue). While the importance of surface chemistry is undeniable, our present experimental equipment does not allow us to go further than to report the experimental procedure and the results. In our experiments, the wetting line of drops remains circular (within experimental error) – no substantial deviation from circular shape is observed.

The typical size of the drops is 4.828 μl for water and 3.200 μl for isopropanol. The experiments are carried out repeatedly to ensure reproducibility. In each experiment, the drop is deposited on a new wafer location. The drops evaporate spontaneously, and the temperature of solid wafers is not controlled. Figures 3(*b*)–3(*d*) show three images recorded during evaporation of a 4.828 μl drop of water. With the exception of a brief interval (<2 s) immediately following the deposition, the evolution of the drop profile is rather slow. We neglect the short initial stage of evolution and concentrate on subsequent dynamics only. Hence, in our discussion below, $t = 0$ refers to the time instant approximately 2 s after drop deposition. The images are recorded at 8 s intervals. The software analyses each image by first verifying that the drop satisfies the spherical cap shape. To this end, a curve is fitted to the drop profile, with maximum permitted average deviation of 1 μm. The data for the radius and the height of the drop at time t_k, R_k and H_k, respectively, are extracted at a cost of the additional error associated with the pixel size, not exceeding 10 μm. The apparent contact angle $\Theta(t_k) = \Theta_k$ is calculated using simple geometrical arguments at the intersection of the liquid–solid interface and the fitted curve, thereby circumventing the pixel-counting procedure and the associated error. Using the data for radius, height and contact angle, we calculate the drop volume V_k and the surface area S_k, based on the spherical cap approximation.

Figure 4(*a*) shows typical evolution of the radius and volume of the evaporating water drop. Consistent with previous works (Deegan 2000; Hu & Larson 2002; Girard *et al.* 2006; Kim *et al.* 2007; Sodtke, Ajaev & Stephan 2007; Girard, Antoni & Sefiane 2008), we observe a linear decrease of volume for the considered time interval. However, we find neither contact line pinning nor significant stick-slip motion, as in Hu & Larson (2002). The lack of contact line pinning is likely a consequence of the smoothness of the solid substrates – typical surface roughness of glass slides

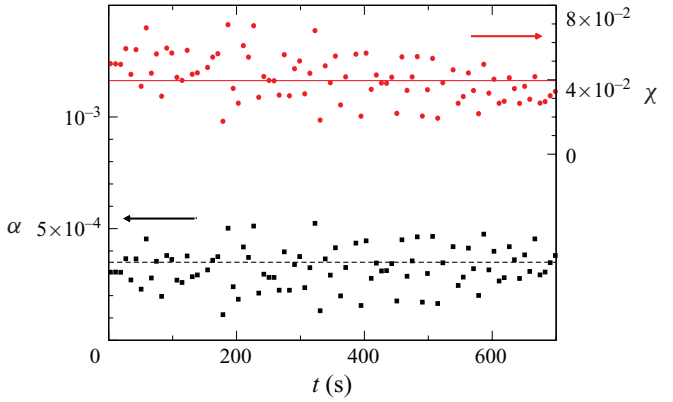

FIGURE 5. (Colour online) Volatility parameters for water. The data points indicate the calculated values and the lines indicate the corresponding average value. The lens model: $\chi = (4.0 \pm 1.2) \times 10^{-2}$. The NEOS model: $\alpha = (3.5 \pm 1) \times 10^{-4}$.

used in Hu & Larson (2002) is $\sim O(1\,\mu\text{m})$, several orders of magnitude larger than the roughness of our Si wafers. Our findings regarding the mobility of the contact line are consistent with the experimental results in Sefiane *et al.* (2008), where similar liquids and solids were used. In addition, in all experiments with water drops, we find that the evolution is characterized by an increasing absolute rate of change of radius, in qualitative agreement with the recent experiments by Sodtke, Ajaev & Stephan (2008), involving water drops in contact with their vapour.

Figure 4(*a*) also indicates that during the final phase of evaporation ($t > t_f = 700\,\text{s}$), when drop thickness is very small, the accuracy of our data deteriorates significantly. This feature is due to the difficulties the software encounters during the curve-fitting process on very thin drops. For this reason, we use only the data obtained for $t < t_f$. Some results of our computations are also compared at an intermediate time, $t_{int} = 106.7\,\text{s}$.

Figure 4(*b*) shows typical variation of Θ during the time interval $[0, t_f]$. We include this variation in our model by using $\Theta(t)$ as given by the linear fit to the experimental data with the slope $-3.26 \times 10^{-2}\,\text{s}^{-1}$ (the line in figure 4*b*). This variation of $\Theta(t)$ suggests that there is the additional resistance to the contact line motion, not included in the model. We leave detailed understanding of this effect for future work and here simply include its effect by using the time-varying coefficient A in (3.1). We note that our approach differs from previous works, such as Ajaev (2005); here contact angle behaviour is directly prescribed by the experiment.

The procedure used to calculate χ and α from the experimental data (volume and surface area) for water drops is described in the Appendix. Figure 5 shows the values of χ and α over the time interval $[0, t_f]$. An important observation is that although there is some spread in the results, χ and α remain constant throughout the considered time interval, as also confirmed by additional experiments with the same size drops. The influence of the initial drop size on these quantities is discussed later in § 6.3.

The relatively small values of α are consistent with those in Mansfield (1955), Derjaguin *et al.* (1966) and Marek & Straub (2001) for water. For example, using the calculation technique and the experimental data for pure water drops without imposed monolayers from Derjaguin *et al.* (1966), we consistently find $\alpha \approx 2 \times 10^{-4}$. Furthermore, our results are in direct agreement with experimentally measured values listed in Barnes (1978). The possibility of having rather small

accommodation coefficient has also been suggested by other authors (e.g. see Colinet *et al.* 2001; Cazabat & Guena 2010). Therefore, such small values are not surprising for water drops evaporating spontaneously in free atmosphere, although they are very different from the ones used in some recent works (e.g. Sultan *et al.* 2005; Sodtke *et al.* 2008). We also note that the obtained values for χ are consistent with those from Guena, Poulard & Cazabat (2007*b*).

In light of the discussion from § 2 regarding the three resistances to evaporation, we note that the obtained value of α yields $\mathscr{R}_p \approx 7.7$. Independently of the relevant thickness l, this value of $\mathscr{R}_p$ is an order of magnitude larger than $\mathscr{R}_c$. However, without knowing l, the relationship between the magnitudes of $\mathscr{R}_p$ and $\mathscr{R}_d$ is unclear. Therefore, the value of α alone is not sufficient to decide which of the two evaporation models (if any) is appropriate. The information regarding the relevant thickness l is likely encoded into the calculated value of χ, and so the natural manner to proceed is to compare the predictions of the two models directly, and against the experimental data.

Finally, we ensure the quality of our experimental data for water through a comparison with the experimental results from Hu & Larson (2002). In particular, we use their data for evaporation of a small water drop on a glass cover slip, with pinned contact line. We apply the same procedure as above and obtain $\chi = 5.1 \times 10^{-2}$ and $\alpha = 3.1 \times 10^{-4}$. Despite the differences in experimental set-ups, these values are in excellent agreement with the results for χ and α obtained from our experiments. Therefore, we have an independent confirmation that our experimental results are reasonably accurate.

In the case of isopropanol, drops become very thin rather quickly, a regime for which the goniometer set-up is ill-suited. Therefore, we use a different approach for calculating χ and α, discussed in § 6.

6. Numerical simulations, comparison with the experimental results and discussion

In order to compare the two evaporation models with the experimental data, we perform numerical simulations of (3.1). Preliminary results of our simulations can be found in Murisic & Kondic (2008). We utilize an extension of the numerical code used in Gotkis *et al.* (2006) to cylindrical geometry. For computational reasons, we carry out simulations using the value of d_{equil} which is larger than in experiments, or in Ajaev (2005) and Sodtke *et al.* (2008), where a different approach to inclusion of vdW forces was employed. However, we have verified that for a sufficiently small value (we use $d_{equil} = 0.625\,\mu$m), there is no influence of this quantity on the evolution of the drop radius. First, we focus on water and carry out simulations using volatility parameters from § 5. Numerical results for the evolution of the contact line position and volume are compared to experimental data, while the results for interface temperatures are compared directly between the two models. Next, we consider isopropanol and describe the method used to calculate the corresponding volatility parameters.

6.1. *Water drops*

For water, the initial condition for simulations matches the experimental data for the corresponding drop immediately after deposition ($R = 2.069$ mm, $H = 0.692$ mm and $\Theta = 41^\circ$). We note that the validity of lubrication approximation even for such large values of Θ has been confirmed by finite element-based simulations in Hu & Larson (2002). The initial condition is developed from a spherical cap profile, evolved for

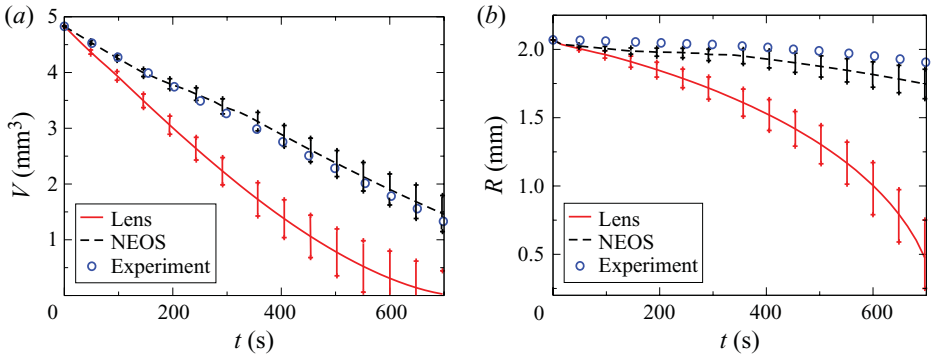

FIGURE 6. (Colour online) Comparison of numerical and experimental results for water. The lines are obtained using the mean values of volatility parameters, shown in figure 5; the error bars correspond to those obtained using the mean values $\pm$ standard deviation; the size of circles shows the experimental error. (a) Evolution of the drop volume and (b) evolution of the contact line position.

a short time using the $J=0$ version of our numerical code in order to ensure its smoothness.

Figure 6(a) shows the volume evolution of the evaporating drop. For this configuration, we find excellent agreement between the experimental results and the NEOS model, which is consistent with Sodtke *et al.* (2008). The lens model overestimates the volume loss, predicting an early dryout at $t=698$ s. The most probable reason for the difference between these results and the earlier work (e.g. Hu & Larson 2002, 2005a,b) is that here, no contact line pinning occurs. The importance of the pinning is in the following: with drop radius fixed, the evaporative mass loss is manifested solely through the thinning of the drop; hence, the variation in Θ is much larger than the one considered here, causing accordingly a larger variation in λ, thereby affecting the predictions of the lens model. The importance of the pinning effect was emphasized in Girard *et al.* (2008): although good agreement between the experiments with pinned drops and the lens model was found, they noted that this model may not be as appropriate when moving contact lines are considered.

Figure 6(b) shows the results for the evolution of the contact line position for the two models in addition to the experimental results. The differences between the models are as substantial as in figure 6(a). The NEOS model is still in better agreement with experimental results compared to the lens model, but both models overestimate the mobility of the contact line. This issue is further discussed below.

Figure 7 compares the temperature profiles at the liquid–gas interface predicted by the lens and NEOS models at $t=t_{int}$, showing a qualitative difference between the two. As illustrated in figure 8, the lens model predicts significantly larger mass flux in the contact line region, causing a sharp temperature decrease. On the other hand, for the NEOS model, the heat supplied from the solid in this region exceeds the heat lost due to evaporation; consequently, temperature increases as one moves from the centre of the drop towards the contact line. The increase in temperature as one moves towards the contact line is consistent with the previous results using the lens model for similar liquids, evaporating either spontaneously (Hu & Larson 2005b; Ristenpart *et al.* 2007) or on weakly heated solids (Girard *et al.* 2006, 2008) under the pinned contact line assumption. The prediction of the NEOS model agrees with the recent numerical results for a similar model in Sodtke *et al.* (2008). Also, it

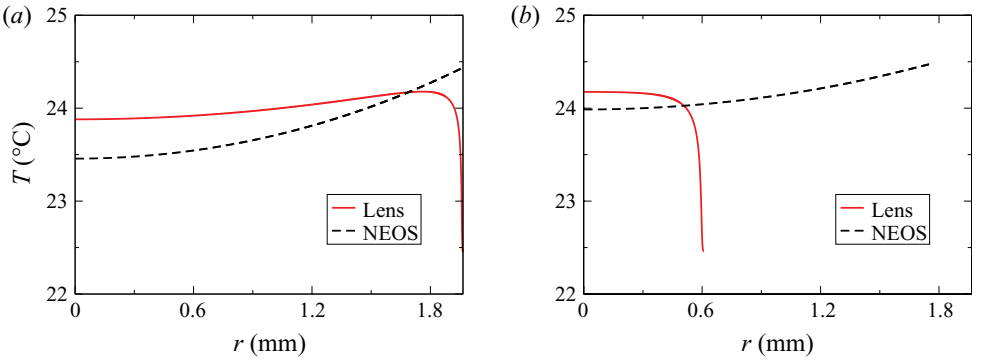

FIGURE 7. (Colour online) Numerical results for water: the temperature of the liquid–gas interface for the lens and NEOS evaporation models. (*a*) At $t = t_{int}$; (*b*) at $t = 681.2$ s. Note the 'stagnation point' in the profile corresponding to the lens model: present at early (*a*), but not at later times (*b*).

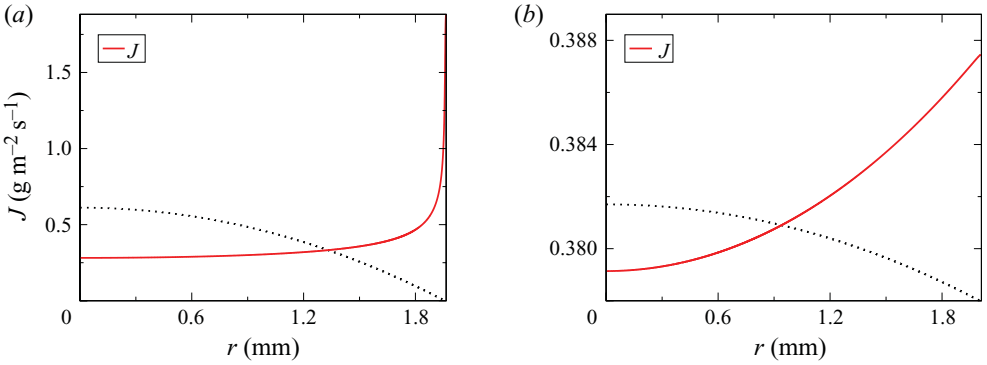

FIGURE 8. (Colour online) Water: mass flux J as a function of the radial coordinate r at $t = t_{int}$. The full lines represent J, and the dotted lines represent the corresponding drop profile at $t = t_{int}$. The labels on the vertical axes correspond to the values of J. (*a*) The lens model. (*b*) The NEOS model.

is consistent with the recent experimental measurements in David, Sefiane & Tadrist (2007), involving a miniature thermocouple, and the ones in Girard *et al.* (2008).

An interesting feature of the results presented in figure 7(*a*) for the lens model is a 'stagnation point' at which temperature gradient changes sign. Similar temperature maximum was proposed as an explanation for the stagnation points recorded experimentally in the flow occurring inside evaporating water drops (Xu & Luo 2007). We note that the non-monotonic temperature profile is not required to understand the experimental results of Xu & Luo (2007): the presence of a stagnation point, based on entirely different physical grounds, was discussed extensively by Deegan *et al.* (2000) and more recently by Berteloot *et al.* (2008), as one of the necessary conditions for the formation of ring-like deposits. We also note that in the lens evaporation model, smaller values of Θ (e.g. at late times as in figure 7*b*) lead to monotonically decreasing temperatures along the liquid–gas interface as one moves away from the drop centre, in full agreement with Hu & Larson (2005*b*) and Ristenpart *et al.* (2007).

Next, we discuss the influence of thermocapillary Marangoni forces within the framework of the model formulated by (3.1). Additional Marangoni forces due to

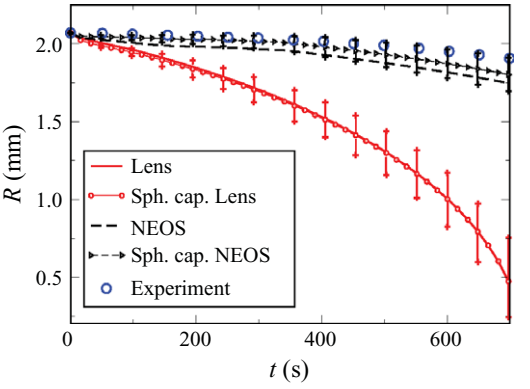

FIGURE 9. (Colour online) Water: $R(t)$ resulting from simulations versus $R_{sph}(t)$, obtained using spherical cap approximation, versus experimental data. Deviation from the spherical cap shape (0.51 % for the lens, 2.33 % for the NEOS model) is defined as the time average of $|R(t) - R_{sph}(t)|/R(t)$. The size of circles indicates the experimental error; error bars on $R_{sph}(t)$ account for the spread in values of χ and α.

the presence of surfactants which may lead to the combined Marangoni effect, as discussed in Hu & Larson (2005*b*), are not considered here. We examine whether thermocapillary Marangoni forces may lead to a deviation from a spherical cap shape, sufficiently large to influence the results in figure 6(*b*) but still below the experimental accuracy. To analyse this possibility, we proceed as follows: at a given time, the numerical result for the thickness at the centre and the corresponding contact angle are both used to calculate the drop radius, assuming the spherical cap shape; this radius is then compared to the one resulting from the simulation. Figure 9 shows that the deviation from the spherical cap shape occurs for both models. Furthermore, the NEOS prediction, modified to satisfy the spherical cap shape, remains very close to the experimental data, when accounted for the spread in the values of α. To confirm that the Marangoni effect is indeed responsible, we carry out additional simulations without gravity ($G = 0$) and find that the influence of gravity is minor. Hence, the distortion from the spherical cap shape due to Marangoni forces may be an important source of the discrepancy in figure 6(*b*). We note in passing that these forces act in opposing directions for the two models, as expected from the temperature profiles in figure 7. In light of the work by Hu & Larson (2005*b*), where it was pointed out that even minor contamination may significantly influence the Marangoni effect, and Xu & Luo (2007), where the thermocapillary Marangoni effect is claimed to be important, it will be of interest to consider the combined thermal/surfactant Marangoni forces in more detail. We leave this issue for future work.

In order to further analyse the influence of the gas phase on evaporation, we carry out additional experiments with mild air current applied by an air ventilator running at moderate speed positioned 3 m away from the experimental set-up. This configuration induces a steady flow in the surrounding gas phase with flow speed $\sim O(1)$ cm s^{-1}. Figure 10 shows the comparison of experimental results for $\bar{J}$, the average evaporative flux, defined as the ratio of the evaporation rate (discussed in the Appendix) and drop surface area. While we see some influence of the additional air current, in particular regarding much larger spread of flux values, this difference does not appear to be statistically significant, at least on the level of our experimental accuracy. This suggests that the evaporation rate is not very sensitive to the manner in which vapour moves away from the interface – vapour motion (diffusion, convection

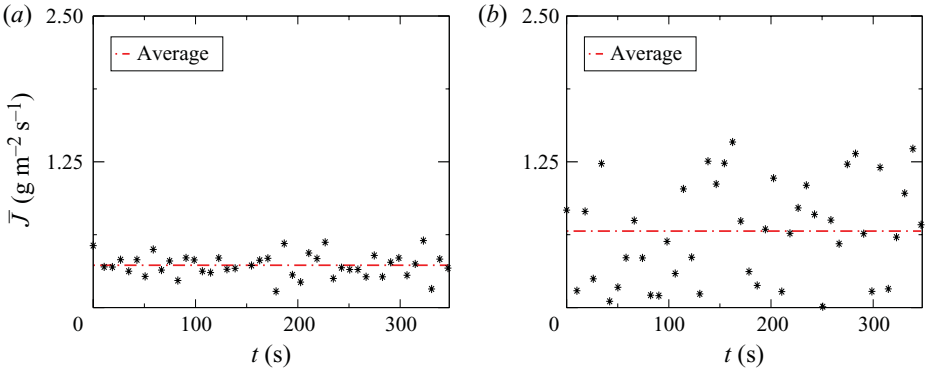

FIGURE 10. (Colour online) Influence of convection on experimentally measured surface-averaged flux $\bar{J}$ for water during the time interval [0, 350 s]. The stars indicate experimental measurements, the dashed lines indicate the corresponding average values. (*a*) Convection-free: $\bar{J} = 0.4 \pm 0.1\,\mathrm{g\,m^{-2}\ s^{-1}}$; (*b*) convected: $\bar{J} = 0.7 \pm 0.4\,\mathrm{g\,m^{-2}\,s^{-1}}$.

or combination of the two) does not appear to be the main factor limiting the evaporation process.

In conclusion, at least for the drop size and set-up considered here, the lens model appears to overestimate both the mass loss and the contact line mobility of water drops with moving contact lines on Si substrates. Here we note that modifications of the lens model, e.g. inclusion of non-stationary effects in the gas (see Poulard, Benichou & Cazabat 2003; Poulard *et al.* 2005), may improve its predictions. The NEOS model describes both the mass loss and the contact line mobility reasonably well. Our results confirm the expectations for spontaneously evaporating water drops, briefly outlined in Cazabat & Guena (2010). Nevertheless, the real verification of the NEOS model should come from the direct measurements of the temperature of the liquid–gas interface, since the two models predict qualitatively different temperature profiles. As we shall see in the next section, this decisive experiment will be even more relevant for the isopropanol case.

6.2. *Isopropanol drops*

Next, we apply the two evaporation models to a more volatile isopropanol. Since this configuration is characterized by a small (apparent) contact angle ($\Theta \sim 6^\circ$ is obtained via the procedure discussed in § 5), in our experiments carried out using the goniometer, we are unable to accurately follow the evolution, since the drop quickly becomes very thin. For this reason, we also carry out experiments using a microscope and a high-speed camera set-up, allowing a view from above and the extraction of the maximum radius achieved by a drop. These experiments and corresponding simulations are discussed in § 6.2.2. We note that all the experiments are carried out in the open atmosphere, so some degree of absorption of water vapour by the isopropanol drop may occur. This absorption may be rapid, but for moderate water intake it leads to only small changes in surface tension. Due to the short duration of the experiments discussed below, we do not expect that absorption has a significant effect on the results. Carrying out experiments in dry air would be of interest if this effect is to be analysed in more detail. While we are not able to monitor experimentally the contact angle evolution, we expect that the relative change in Θ is small, as expected for the configurations characterized by spontaneous evaporation, where contamination of the free surface is not as important as for water, the liquid

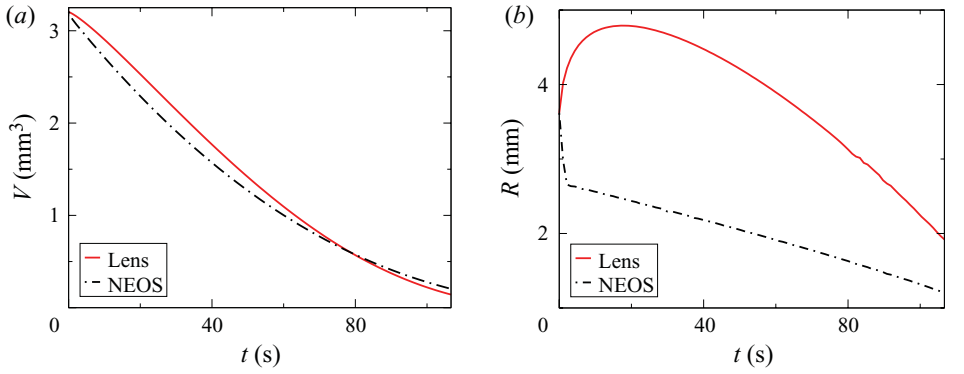

FIGURE 11. (Colour online) Comparison of numerical results for isopropanol for the lens and NEOS models. Time interval: $[0, t_{int}]$. (*a*) Evolution of the drop volume; (*b*) evolution of the contact line position, see Murisic & Kondic (2008).

is partially wetting and the contact line speed is moderate, see e.g. Cazabat & Guena (2010).

Immediately upon deposition ($t < 1$ s), we observe fast spontaneous spreading of isopropanol drops. Similarly as for water, we ignore this phase and focus on subsequent evolution. Although in our experiments with goniometer we are not able to collect as extensive data as for water, we can extract initial profiles and the dryout time with reasonable accuracy (estimated error $\leqslant 10\,\%$). In particular, for $V_0 = 3.200\,\mu$l, we consistently find $t_{dry} \approx 125$ s. We use this dryout time to obtain the volatility parameters: requiring that the dryout times in the simulations match the experimentally measured one yields $\chi = 5.7 \times 10^{-3}$ and $\alpha = 9.3 \times 10^{-4}$ (here, we do not consider the time dependence of Θ). Similar values of χ were obtained in the experiments with pure alkanes in Guena *et al.* (2007*b*), while the value of α is consistent with the experimentally measured values for water/alcohol mixtures (Barnes 1978). We note that the values of χ and α estimated in this manner do not exhibit any significant dependence on the initial profile used in simulations.

Next, we consider briefly the argument concerning resistances. The calculated value of α yields $\mathscr{R}_p \approx 0.56$, an order of magnitude larger than $\mathscr{R}_c$. The value of $\mathscr{R}_d$ depends on l: $\mathscr{R}_d \approx 0.05$, 0.54 and 43 for $l = 0.1d_0$, d_0 and $80d_0$ respectively. Therefore, since the answer regarding the dominant resistance again depends on the value of l, we proceed with the numerical simulations of (3.1). In what follows, we compare the predictions of the lens and NEOS models directly, to our experimental results and also to Cachile *et al.* (2002), Poulard *et al.* (2005) and Guena, Allancon & Cazabat (2007*a*). The initial condition for our simulations (unless otherwise noted) corresponds to an experimentally measured profile immediately after the deposition ($R = 3.723$ mm, $H = 0.147$ mm and $\Theta = 6°$). A smooth initial condition is developed in the same manner as for water.

Figure 11(*a*) shows the numerical results for the evolution of volume for the two evaporation models. The agreement between the lens and the NEOS model is not surprising since the volatility parameters χ and α have been estimated from experimentally measured t_{dry}. On the other hand, figure 11(*b*) shows dramatically different contact line evolutions. Figure 12 shows the temperature profiles at the liquid–gas interface and provides immediate understanding of the results in figure 11(*b*). The Marangoni forces act in the opposing directions for the lens and NEOS models. For the lens model, they are directed outwards, leading to an initial

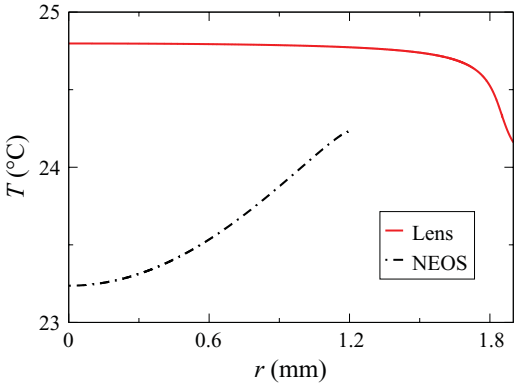

FIGURE 12. (Colour online) Isopropanol: the temperature of the liquid–gas interface at $t = t_{int}$ for the two models, see Murisic & Kondic (2008).

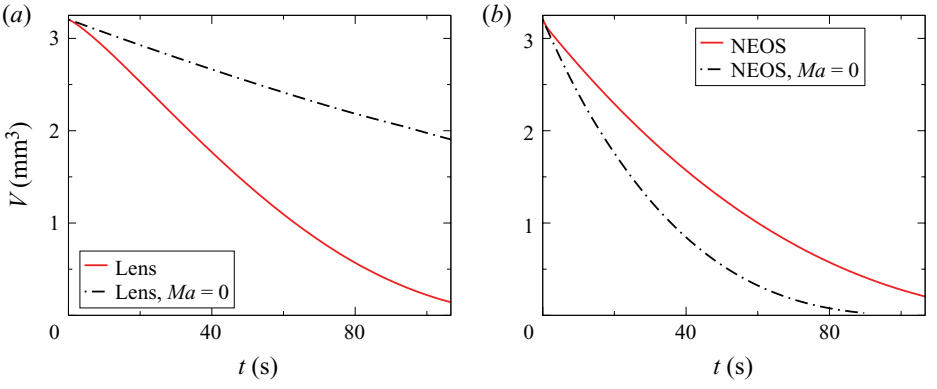

FIGURE 13. (Colour online) Volume evolution for isopropanol with and without Marangoni forces for the time interval $[0, t_{int}]$. (*a*) The lens model. (*b*) The NEOS model.

spreading, in spite of the mass loss due to evaporation. The difference between the temperature profiles for the two evaporation models is much more pronounced for isopropanol compared to water, due to its larger volatility. We also note that in contrast to water, the lens model for isopropanol exhibits monotonically decreasing temperature along the liquid–gas interface. This is due to the increased volatility and smaller Θ, in agreement with Hu & Larson (2005*b*).

6.2.1. *Role of Marangoni forces*

In order to gain even better understanding of the role of Marangoni forces, we carry out simulations where the Marangoni effect is switched off by setting $Ma = 0$. Figures 13 and 14 show the evolution of volume and radius, with and without Marangoni forces. Figure 13 confirms that Marangoni forces significantly affect the mass loss for both models – setting $Ma = 0$ leads to a *decrease* (an *increase*) in the rate of mass loss for the lens (NEOS) model. This effect is particularly pronounced for the lens model, where a substantial reduction in the mobility of the contact line also occurs, see figure 14(*a*). Figure 14(*b*) shows that the exclusion of Marangoni forces in the NEOS model prevents the swift initial receding motion.

An explanation of these results is as follows. For the lens model, Marangoni forces lead to a strong outward flow close to the contact line, due to large temperature

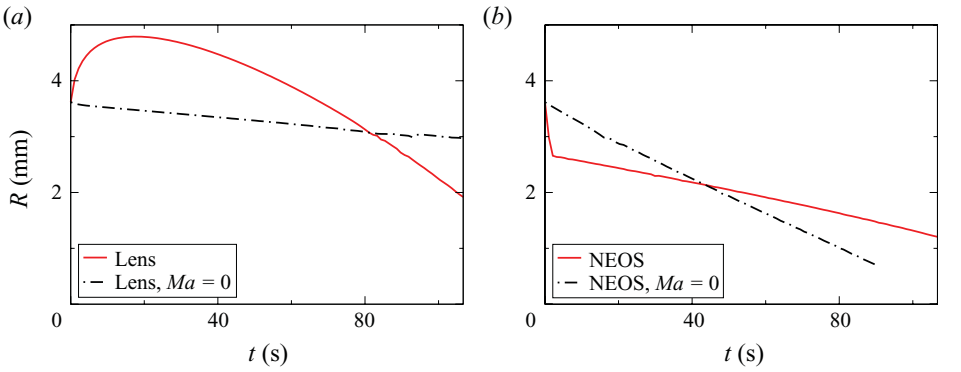

FIGURE 14. (Colour online) Radius evolution for isopropanol with and without Marangoni forces for the time interval $[0, t_{int}]$. (*a*) The lens model. (*b*) The NEOS model.

gradient there. The liquid in the vicinity of the contact line is being propelled outwards, forming a thin stretched layer. Initially, the liquid lost due to evaporation from this 'super'-volatile thin zone is replenished by the liquid from the bulk. However, this process cannot be sustained, and eventually the receding phase sets in. When Marangoni forces are neglected, no initial spreading occurs, see figure 14(*a*). Without the rapid increase in the surface area, the evaporation rate declines sharply. Since the receding motion is entirely due to the mass loss, this decrease in the evaporation rate causes slower receding motion.

For the NEOS model, the Marangoni induced flow along the liquid–gas interface is inward and uniform (unlike for the lens model, where it is most pronounced close to the contact line). It causes rapid receding motion shown in figure 14(*b*). As a result, the surface area of the drop is decreased, leading to slower evaporation. When $Ma = 0$, the swift initial receding motion is suppressed. Therefore, the rapid decrease in the surface area is prevented and the evaporation rate is larger, causing overall faster receding motion.

6.2.2. *Comparison to experimental data*

The lens model predicts two distinct phases in the evolution: swift initial spreading followed by receding motion, see figure 11(*b*). Qualitatively similar behaviour occurred in experiments with alkanes of similar volatility in Cachile *et al.* (2002). In Poulard *et al.* (2005) and Guena *et al.* (2007*a*), the dependence of the maximum extent of spreading, R_{max}, on the initial drop volume, V_0, in the range [0.01 µl, 10 µl] was studied experimentally for alkanes. They found a power law dependence, $R_{max} = C_a V_0^{C_b}$, where $C_a \approx 3$ and $C_b = 0.4$. For the purpose of comparison, we carry out additional simulations, where we record R_{max} for few initial drop volumes. The parameter values are the same as before, with the exception of χ and α, which are re-evaluated from dryout times for each considered V_0 (dependence of χ and α on V_0 is discussed in § 6.3). Here, we use hemispherical initial conditions, $\Theta(0) = 90°$, in order to more realistically simulate the profiles at the deposition time. Figure 15(*a*) compares our numerical results with a power law (the 'Slope 0.4' line). It shows that both evaporation models exhibit a power law behaviour with exponent ≈0.4. Furthermore, $R_{max} = 3V_0^{0.4}$ fits the lens results almost exactly, which is in excellent agreement with Poulard *et al.* (2005) and Guena *et al.* (2007*a*).

As mentioned above, we have carried out additional experiments using a microscope and high-speed camera set-up to measure the diameter of isopropanol drops. A syringe

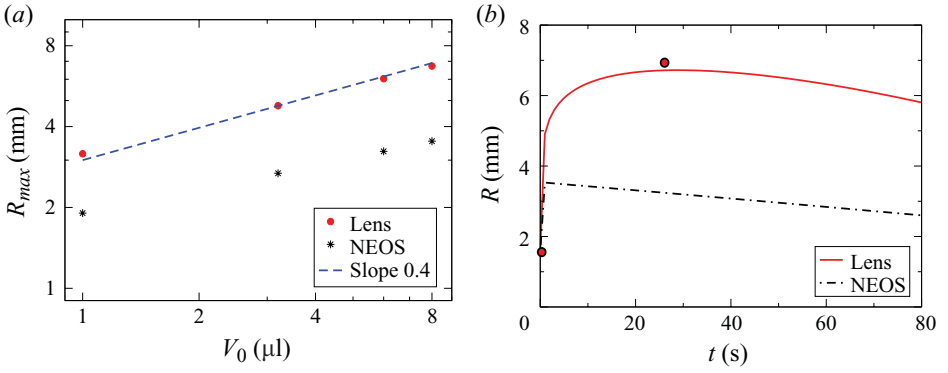

FIGURE 15. (Colour online) (*a*) Numerical results for isopropanol: maximum extent of spreading versus initial drop volume. Line 'Slope 0.4' corresponds to $R_{max} = 3V_0^{0.4}$; $V_0 =$ 1.000, 3.200, 6.000 and 8.000 μl; (*b*) isopropanol: evolution of the contact line position for the two evaporation models. The initial condition is a 7.900 μl hemisphere. The circles indicate experimental data for $(0, R(0))$, $(t_{max}, R(t_{max}))$.

is used to manually deposit ≈7.900 μl drops of isopropanol, and then the position of the contact line is tracked. We find that the maximum radius of ≈7.000 mm is achieved 25.0 s after the deposition. We then perform numerical simulations for both evaporation models, again using the hemispherical initial condition. Figure 15(*b*) shows that the maximum radius, $R_{max} = 6.720$ mm, for the lens model is achieved at 26.9 s, which is in excellent agreement with the experimental data. On the other hand, the NEOS model substantially underestimates the contact line mobility. These results support the conclusions of § 6.2.1 regarding the role of Marangoni forces. Definite confirmation of this hypothesis lies in the experiments with the saturated gas phase, which are left for future work.

In view of the results presented so far, it appears that, at least for the considered drop size and set-up, the lens model more realistically describes the evaporation of a more volatile liquid, here isopropanol. We discuss below several reasons why such an outcome is not surprising. Here, we note that this result is further supported in Sefiane *et al.* (2008), where the spontaneous evaporation of water/methanol mixtures with volatility comparable to isopropanol and moving contact lines was studied; although evaporation of mixtures may not be best described by a model based on spherical cap approximation, it was found that the predictions of the lens model are in excellent agreement with the experiments. This outcome is also supported by a recent discussion on the applicability of the lens model given in Cazabat & Guena (2010).

6.3. *Influence of drop volume*

Here, we discuss the influence of the initial drop volume. Recall the argument from § 2 that the evaporative flux, ignoring the effect of heat conduction in liquid (and solid, i.e. $\mathscr{W} = 0$), may be written as $J \propto 1/(\mathscr{R}_p + \mathscr{R}_d)$. If one ignores $\mathscr{R}_d$ for a moment, one effectively reduces the flux to the NEOS model, with the liquid thermal conductivity ($\mathscr{R}_c$ term in (2.7) or h in (4.6)) neglected. Effectively, since $\mathscr{R}_p \propto 1/\alpha$, one has the flux in the form

$$J \propto \frac{1}{1/\alpha}. \tag{6.1}$$

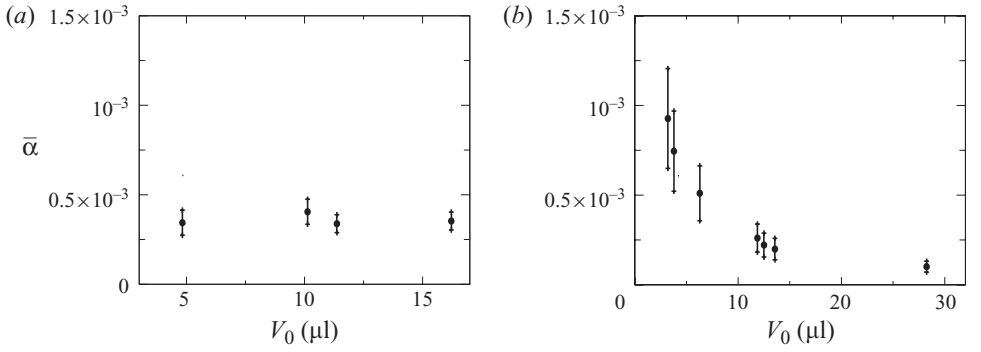

FIGURE 16. Effective accommodation coefficient, $\bar{\alpha}$, versus the initial drop volume. (*a*) Water: $V_0 = 4.828$, 10.129, 11.372 and 16.214 μl; (*b*) isopropanol: $V_0 = 3.200$, 3.785, 6.287, 11.865, 12.506, 13.561 and 28.244 μl. Average values (circles) $\pm$ standard deviation are plotted; deviation in (*b*) is based on the error in measured t_{dry} ($\leqslant 10\,\%$).

Allow now for a possibility that $\mathscr{R}_d$ plays a role. $\mathscr{R}_d$ is proportional to the ratio $l/d_0 = \delta$, and one expects that δ is an increasing function of the drop size, see Haut & Colinet (2005). One can interpret δ as a scaled distance in the gas phase over which vapour concentration changes substantially. We note in passing that particular scaling $\delta \propto \sqrt{d_0}$ and ignoring $\mathscr{R}_p$ leads directly to the lens model in the limit of small contact angle. More generally, one can write $\mathscr{R}_d = f(V_0)$, where $f(V_0)$ is some monotonically increasing function of the initial drop volume, V_0. Adding this contribution to the flux leads to

$$J \propto \frac{1}{f(V_0) + 1/\alpha} = \frac{1}{1/\bar{\alpha}}, \tag{6.2}$$

which defines the 'effective' accommodation coefficient, $\bar{\alpha}$. Hence, if the diffusion of vapour in the gas influences evaporation, one expects that $\bar{\alpha}$ depends on V_0.

To explore this possibility for water, we carry out additional experiments with a few different initial volumes, calculating $\bar{\alpha}$ in the manner described in § 5. Figure 16(*a*) shows that the obtained values of $\bar{\alpha}$ *do not* vary with V_0, at least within the range of drop sizes achievable using available experimental equipment. Therefore, we conjecture that any process which depends on the initial drop size is not dominant in the water experiments considered here, supporting the rest of the results presented in this paper.

Next we consider isopropanol using the same approach as in § 6.2. Figure 16(*b*) shows the values of $\bar{\alpha}$ obtained for the drops within the range [3.200 μl, 28.244 μl]. Here, we find that $\bar{\alpha}$ *does* strongly depend on the drop size, suggesting that the diffusion of vapour into surrounding gas has an important effect. In particular, the fact that $\bar{\alpha}$ is a decreasing function of the drop volume is in agreement with the qualitative argument presented above.

7. Conclusions

Evaporation in the presence of moving interfaces and contact lines is a complicated problem. The presence of multiple phases and multiple scales, including very short ones in the vicinity of fronts, leads to complex formulations which need to be simplified. The simplifications are often difficult to justify due to unknown values of physical parameters. In this paper we have shown that two commonly used

evaporation models resulting from such simplifications lead to qualitatively different results, including drop evolution and thermal gradients along the liquid–gas interface.

Our extensive review of the literature illustrates both the necessity of development of simplified models and difficulties in reaching them. It serves to clearly identify the governing parameters strongly influencing the simplification path which should be taken: the accommodation coefficient, governing molecular transport across the interface and the relevant extent of the gas phase. Both may vary in experiments and applications. This encouraged us to carry out our own experiments, use the obtained data to extract the unknown accommodation coefficient and simulate drop evolution. The procedure we use has effectively allowed for a direct comparison between the predictions of the two evaporation models corresponding to a particular physical set-up. To our knowledge, this is the first implementation of such an approach.

The evaporation is embedded into the model based on the long-wave theory, formulated to allow for time-dependent simulations of drop evolution. This model includes capillary, thermal and body forces, as well as the interaction with the solid, via the disjoining pressure approach. The key quantity, evaporative flux, is kept in the formulation explicitly, see (3.1), so that one can easily default to any desired functional form. The experiments, carried out with deionized water and isopropanol on smooth silicon wafers, are then used to extract the needed volatility parameters. The resulting values of the accommodation coefficient are $\approx 3.5 \times 10^{-4}$ for water and 9.3×10^{-4} for more volatile isopropanol; although substantially smaller than the ones used recently, they are consistent with the experimental values in the literature. The results of our simulations and their comparison with the experiments show how strongly the material parameters influence the evaporation process. For water, we find that a model (the NEOS) with the evaporative flux based on the liquid effects agrees well with the experiments; for more volatile isopropanol, the lens model, concentrating on the gas phase, is in much better agreement.

The simulations are then used to clearly show the importance of various physical effects. In particular, they are carried out with and without Marangoni stresses, showing that the thermal effects are significant, and can influence the evolution even in the case of a slowly evaporating water drop at the room temperature. For isopropanol, the role of these stresses in determining the evolution is even more significant. Our results also suggest that the thermal effects are particularly relevant to the configurations such as those considered here, where evolution proceeds without contact line pinning. The differences between our results and those from works focusing on pinned cases serve to highlight the importance of the front mobility. More precisely, it releases the stresses there, so that only a minor change in the apparent contact angle due to evaporation occurs, in contrast to the pinned case. Evaporation may have much stronger influence if contact line motion is allowed, since non-uniform evaporation leads to Marangoni stresses which directly influence the contact line dynamics.

In the last part of the paper, we discuss, in qualitative terms, the foundations of a more general approach which would include aspects of both models discussed extensively in this work. In particular, we show that the diffusion of vapour in the gas, if relevant to evaporation, leads to an 'effective' accommodation coefficient that depends on the initial drop volume. Further experiments have confirmed that this dependence is absent for water, suggesting that the NEOS model is indeed applicable. However, for isopropanol, we find that this quantity does depend on the initial drop volume, suggesting that the diffusion of vapour is important, consistent with all the other presented results. Future work should include much more careful treatment of

evaporation next to the contact line in the presence of a vapour/inert gas mixture. New asymptotic methods will also need to be developed to connect the nano-scale of relevance to the contact line physics and the macro-scale of a drop. Until this is done, the obtained results suggest that significant care is required when deciding which approach to use in modelling evaporation. In particular, the difference in temperature profiles at the liquid–gas interface for the two models suggests that the arguments concerning the influence of the Marangoni forces on the formation of particle deposits next to the contact line may have to be carefully re-examined. More elaborate experiments, involving the measurement of the temperature at the liquid–gas interface, are therefore necessary, as they will provide an ultimate criterion for the selection of an appropriate evaporation model.

The authors acknowledge many insightful conversations with Pierre Colinet and Alex Rednikov, and thank Yehiel Gotkis, PhD, a former KLA-Tencor Corp. and Lam Research Corp. scientist, for introducing us to many interesting problems involving evaporation. The support by Katrina Mikhaylich, PhD, and Lam Research Corporation for donating Si wafers is gratefully acknowledged. The equipment used in the experiments was partially funded by the NSF CCLI grant no. 0511514.

Appendix

Here we show the procedure used to extract the volatility parameters, χ and α, from the experimental data. First, we calculate the evaporation rate $J_k^{rate} = \rho \Delta V_k / \Delta t_k$, valid for each time interval $[t_k, t_{k+1}]$, where $\Delta V_k = V_k - V_{k+1}$ and $\Delta t_k = t_{k+1} - t_k$. This evaporation rate corresponds to the surface integral of $J^*(h^*)$, calculated over the drop surface recorded in the experiment at time instant t_{k+1}. The drop surface is assumed to be well approximated by a spherical cap. In calculating surface integrals, we use either (4.3) for the lens or (4.6) for the NEOS model. To be consistent with our numerical simulations, we integrate down to the thickness of equilibrium film, d_{equil}. The evaporation rate does not depend on d_{equil} in any significant manner, as discussed earlier.

The surface integral of the mass flux $J^*(h^*)$ is given by

$$J_k^{rate} = \int_{S_{k+1}} J^* \, \mathrm{d}S^* = \int\int J^*(\boldsymbol{\varrho}^*) \left[\frac{\partial \boldsymbol{\varrho}^*}{\partial x^*} \times \frac{\partial \boldsymbol{\varrho}^*}{\partial y^*} \right] \mathrm{d}x^* \, \mathrm{d}y^*. \tag{A 1}$$

Here, S_{k+1} is the surface of the drop at time t_{k+1}. The quantity multiplying $J^*(\boldsymbol{\varrho}^*)$ in the double integral is a Jacobian, where $\boldsymbol{\varrho}^* = (x^*, y^*, z^*)$, and $z^* = f_k(x^*, y^*) = \sqrt{B_k{}^2 - (x^{*2} + y^{*2})} - d_k + d_{equil}$ is the spherical cap at time t_k (i.e. B_k and d_k are B and d from figure 2 at time t_k). Equation (A 1) can be rewritten in the following form:

$$J_k^{rate} = \int\int J^*(f_{k+1}) \sqrt{1 + \left(\frac{\partial f_{k+1}}{\partial x^*} \right)^2 + \left(\frac{\partial f_{k+1}}{\partial y^*} \right)^2} \, \mathrm{d}x^* \, \mathrm{d}y^*. \tag{A 2}$$

Similar expressions for the evaporation rate were used previously (e.g. see Deegan *et al.* 2000; Hu & Larson 2002). For sufficiently thin drops, i.e. complete wetting case, (A 2) simplifies to an integral over drop's circular base (see e.g. Poulard *et al.* 2003; Dunn *et al.* 2008, 2009); clearly, such simplification is not applicable to liquid/solid configurations considered here. Also, unlike in e.g. Poulard *et al.* (2005), here, no

additional regularization of J^* is needed, since our model includes the attractive liquid–solid forces.

For the lens model, the dimensional version of (4.3) is substituted into (A 2), which is then rewritten in polar coordinates. We define χ_k^* as a dimensional equivalent of the volatility parameter χ at time t_k. By treating χ_k^* as a constant for each interval $[t_k, t_{k+1}]$, we find

$$J_k^{rate} = 2\pi B_{k+1} I_{l,k+1} \chi_k^*, \tag{A 3}$$

where $I_{l,k+1}$ is the following integral:

$$I_{l,k+1} = \int_0^{R_{k+1}} \frac{r^* \, \mathrm{d}r^*}{\sqrt{{B_{k+1}}^2 - r^{*2}} \left(\sqrt{{B_{k+1}}^2 - r^{*2}} - d_{k+1} + d_{equil} \right)^{\psi}}, \tag{A 4}$$

which is calculated numerically for each k. We can therefore calculate χ valid for the interval $[t_k, t_{k+1}]$: $\chi_k = \chi_k^* / (d_0^{\psi}[J])$, with $[J]$ defined in § 4. Finally, since ψ is a function of the contact angle Θ, the values of Θ used in calculating χ match those used for solving (3.1) numerically. In view of the arguments in § 4 regarding ψ, we use $\psi = \lambda$ for water, with the expression for λ taken from Hu & Larson (2002).

For the NEOS model, the dimensional version of (4.6) is the appropriate expression for $J^*(h^*)$. The procedure similar to the one described for the lens model gives

$$J_k^{rate} = 2\pi d_0 [J] B_{k+1} I_{N,k+1}(\alpha_k), \tag{A 5}$$

where $I_{N,k+1}(\alpha_k)$ is the following integral:

$$I_{N,k+1}(\alpha_k) = \int_0^{R_{k+1}} \frac{r^* \, \mathrm{d}r^*}{\sqrt{{B_{k+1}}^2 - r^{*2}} \left(d_0(\mathscr{K}(\alpha_k) + \mathscr{W}) - d_{k+1} + d_{equil} \right) + {B_{k+1}}^2 - r^{*2}}. \tag{A 6}$$

Here, $\mathscr{K}$, given by (4.5), is treated as a function of the unknown volatility parameter, $\mathscr{K} = \mathscr{K}(\alpha_k)$. The problem of solving for α_k is recast into a minimization problem $\alpha_k = \min_{\alpha_k \in [10^{-6}, 1]} \Gamma(\alpha_k)$, where $\Gamma(\alpha_k)$ is defined as

$$\Gamma(\alpha_k) = \left| \frac{J_k^{rate}}{2\pi d_0 [J] B_{k+1}} - I_{N,k+1}(\alpha_k) \right|, \tag{A 7}$$

which is solved numerically for all k.

REFERENCES

Ajaev, V. S. 2005 Spreading of thin volatile liquid droplets on uniformly heated surfaces. *J. Fluid Mech.* **528**, 279.

Anderson, D. M. & Davis, S. H. 1995 The spreading of volatile liquid droplets on heated surfaces. *Phys. Fluids* **7**, 248.

Atkins, P. & de Paula, J. 2006 *Atkins' Physical Chemistry*, 8th edn. Oxford University Press.

Barash, L. Yu., Bigioni, T. P., Vinokur, V. M. & Shchur, L. N. 2009 Evaporation and fluid dynamics of a sessile drop of capillary size. *Phys. Rev.* E **79**, 046301.

Barnes, G. T. 1978 Insoluble monolayers and the evaporation coefficient for water. *J. Colloid Interface Sci.* **65**, 5666.

Barnes, G. T. 1986 The effects of monolayers on the evaporation of liquids. *Adv. Colloid Interface Sci.* **25**, 89.

Berteloot, G., Pham, C. T., Daerr, A., Lequeux, F. & Limat, L. 2008 Evaporation-induced flow near a contact line: consequences on coating and contact angle. *Europhys. Lett.* **83**, 14003.

Bhardwaj, R., Fang, X. & Attinger, D. 2009 Pattern formation during the evaporation of a colloidal nanoliter drop: a numerical and experimental study. *New J. Phys.* **11**, 075020.

Blossey, R. 2003 Self-cleaning surfaces – virtual realities. *Nature Mater.* **2**, 301.

Burelbach, J. P., Bankoff, S. G. & Davis, S. H. 1988 Nonlinear stability of evaporating/condensing liquid films. *J. Fluid Mech.* **195**, 463.

Cachile, M., Benichou, O., Poulard, C. & Cazabat, A. M. 2002 Evaporating droplets. *Langmuir* **18**, 8070.

Cammenga, H. K. 1980 Evaporation mechanisms of liquids. In *Current Topics in Materials Science* (ed. E. Kaldis), vol. V/4, p. 335. North-Holland.

Cazabat, A. & Guena, G. 2010 Evaporation of macroscopic sessile droplets. *Soft Matter* **6**, 2591.

Clausius, R. 1850 Über die bewegende Kraft der Wärme und die Gesetze, welche sich daraus für die Wärmelehre selbst ableiten lassen. *Ann. Phys. Chem.* **79**, 368, 500.

Colinet, P., Legros, J. C. & Velarde, M. G. 2001 *Nonlinear Dynamics of Surface-Tension-Driven Instabilities*. Wiley-VCH.

Craster, R. V. & Matar, O. K. 2009 Dynamics and stability of thin liquid films. *Rev. Mod. Phys.* **81**, 1131.

David, S., Sefiane, K. & Tadrist, L. 2007 Experimental investigation of the effect of thermal properties of the substrate in the wetting and evaporation of sessile drops. *Colloids Surf.* A **298**, 108.

Deegan, R. D. 2000 Pattern formation in drying drops. *Phys. Rev.* E **61**, 475.

Deegan, R. D., Bakajin, O., Dupont, T. F., Huber, G., Nagel, S. R. & Witten, T. A. 1997 Capillary flow as the cause of ring stains from dried liquid drops. *Nature* **389**, 827.

Deegan, R. D., Bakajin, O., Dupont, T. F., Huber, G., Nagel, S. R. & Witten, T. A. 2000 Contact line deposits in an evaporating drop. *Phys. Rev.* E **62**, 756.

Derjaguin, B. V., Fedoseyev, V. A. & Rosenzweig, L. A. 1966 Investigation of the adsorption of cetyl alcohol vapor and the effect of this phenomenon on the evaporation of water drops. *J. Colloid Interface Sci.* **22**, 45.

Diez, J. & Kondic, L. 2007 On the breakup of fluid films of finite and infinite extent. *Phys. Fluids* **19**, 072107.

Dondlinger, M., Margerit, J. & Dauby, P. C. 2005 Weakly nonlinear study of Marangoni instabilities in an evaporating liquid layer. *J. Colloid Interface Sci.* **283**, 522.

Dunn, G. J., Wilson, S. K., Duffy, B. R., David, S. & Sefiane, K. 2008 A mathematical model for the evaporation of a thin sessile liquid droplet: comparison between experiment and theory. *Colloids Surf.* A **323**, 50.

Dunn, G. J., Wilson, S. K., Duffy, B. R., David, S. & Sefiane, K. 2009 The strong influence of substrate conductivity on droplet evaporation. *J. Fluid Mech.* **623**, 329.

Fang, G. & Ward, C. A. 1999 Temperature measured close to the interface of an evaporating liquid. *Phys. Rev.* E **59**, 417.

Fischer, B. J. 2002 Particle convection in an evaporating colloidal droplet. *Langmuir* **18**, 60.

Girard, F., Antoni, M., Faure, S. & Steinchen, A. 2006 Evaporation and Marangoni driven convection in small heated water droplets. *Langmuir* **22**, 11085.

Girard, F., Antoni, M. & Sefiane, K. 2008 On the effect of Marangoni flow on evaporation rates of heated water drops. *Langmuir* **24**, 9207.

Gotkis, Y., Ivanov, I., Murisic, N. & Kondic, L. 2006 Dynamic structure formation at the fronts of volatile liquid drops. *Phys. Rev. Lett.* **97**, 186101.

Guena, G., Allancon, P. & Cazabat, A. M. 2007*a* Receding contact angle in the situation of complete wetting: experimental check of a model used for evaporating droplets. *Colloids Surf.* A **300**, 307.

Guena, G., Poulard, C. & Cazabat, A. M. 2007*b* Evaporating drops of alkane mixtures. *Colloids Surf.* A **298**, 2.

Haut, B. & Colinet, P. 2005 Surface-tension-driven instabilities of a pure liquid layer evaporating into an inert gas. *J. Colloid Interface Sci.* **285**, 296.

Hocking, L. M. 1995 On contact angles in evaporating liquids. *Phys. Fluids* **7**, 2950.

Hu, H. & Larson, R. G. 2002 Evaporation of a sessile droplet on a substrate. *J. Phys. Chem.* B **106**, 1334.

Hu, H. & Larson, R. G. 2005*a* Analysis of the microfluid flow in an evaporating sessile droplet. *Langmuir* **21**, 3963.

Hu, H. & Larson, R. G. 2005*b* Analysis of the effects of Marangoni stresses on the microflow in an evaporating sessile droplet. *Langmuir* **21**, 3972.

Israelachvili, J. N. 1992 *Intermolecular and Surface Forces*, 2nd edn. Academic.

Kennard, E. H. 1938 *Kinetic Theory of Gases with an Introduction to Statistical Mechanics*. McGraw-Hill.

Kim, J., Ahn, S. I., Kim, J. H. & Zin, W. 2007 Evaporation of water droplets on polymer surfaces. *Langmuir* **23**, 6163.

Knudsen, M. 1915 Die maximale Verdampfungsgeschwindigkeit des Quecksilbers. *Ann. Phys.* **47**, 697.

Lide, D. R. (Ed.) 1997 *Handbook of Chemistry and Physics*, 78th edn. CRC Press.

Mansfield, W. W. 1955 Influence of monolayers on the natural rate of evaporation of water. *Nature* **175**, 247.

Marek, R. & Straub, J. 2001 Analysis of the evaporation coefficient and the condensation coefficient of water. *Intl J. Heat Mass Transfer* **44**, 39.

Margerit, J., Dondlinger, M. & Dauby, P. C. 2005 Improved 1.5-sided model for the weakly nonlinear study of Benard–Marangoni instabilities in an evaporating liquid layer. *J. Colloid Interface Sci.* **290**, 220–230.

Morris, S. J. S. 2001 Contact angles for evaporating liquids predicted and compared with existing experiments. *J. Fluid Mech.* **432**, 1.

Murisic, N. & Kondic, L. 2008 Modeling evaporation of sessile drops with moving contact lines. *Phys. Rev.* E **78**, 065301.

Oron, A., Davis, S. H. & Bankoff, S. G. 1997 Long-scale evolution of thin liquid films. *Rev. Mod. Phys.* **69**, 931.

Picknett, R. G. & Bexon, R. 1977 The evaporation of sessile or pendant drops in still air. *J. Colloid Interface Sci.* **61**, 336.

Plesset, M. S. & Prosperetti, A. 1976 Flow of vapour in a liquid enclosure. *J. Fluid Mech.* **78**, 433.

Popov, Y. O. 2005 Evaporative deposition patterns: spatial dimensions of the deposit. *Phys. Rev.* E **71**, 036313.

Poulard, C., Benichou, O. & Cazabat, A. M. 2003 Freely receding evaporating droplets. *Langmuir* **19**, 8828.

Poulard, C., Guena, G., Cazabat, A. M., Boudaoud, A. & ben Amar, M. 2005 Rescaling the dynamics of evaporating drops. *Langmuir* **21**, 8226.

Ristenpart, W. D., Kim, P. G., Domingues, C., Wan, J. & Stone, H. A. 2007 Influence of substrate conductivity on circulation reversal in evaporating drops. *Phys. Rev. Lett.* **99**, 234502.

Schrage, R. W. 1953 *A Theoretical Study of Interphase Mass Transfer*. Columbia University Press.

Schwartz, L. W. & Eley, R. R. 1998 Simulation of droplet motion of low-energy and heterogenous surfaces. *J. Colloid Interface Sci.* **202**, 173.

Sefiane, K., David, S. & Shanahan, M. E. R. 2008 Wetting and evaporation of binary mixture drops. *J. Phys. Chem.* B **112**, 11317.

Sefiane, K. & Ward, C. A. 2007 Recent advances on thermocapillary flows and interfacial conditions during the evaporation of liquids. *Adv. Colloid Interface Sci.* **134**, 201.

Sodtke, C., Ajaev, V. S. & Stephan, P. 2007 Evaporation of thin liquid droplets on heated surfaces. *Heat Mass Transfer* **43**, 649.

Sodtke, C., Ajaev, V. S. & Stephan, P. 2008 Dynamics of volatile liquid droplets on heated surfaces: theory versus experiment. *J. Fluid Mech.* **610**, 343.

Sultan, E., Boudaoud, A. & ben Amar, M. 2005 Evaporation of a thin film: diffusion of the vapor and Marangoni instabilities. *J. Fluid Mech.* **543**, 183.

Xu, X. & Luo, J. 2007 Marangoni flow in an evaporating water droplet. *Appl. Phys. Lett.* **91**, 124102.